Environment and Early Evolution of the 8 May 2009 Derecho-Producing Convective System

MICHAEL C. CONIGLIO

NOAA/National Severe Storms Laboratory, Norman, Oklahoma

STEPHEN F. CORFIDI

NOAA/Storm Prediction Center, Norman, Oklahoma

JOHN S. KAIN

NOAA/National Severe Storms Laboratory, Norman, Oklahoma

(Manuscript received 10 March 2010, in final form 6 October 2010)

ABSTRACT

This study documents the complex environment and early evolution of the remarkable derecho that traversed portions of the central United States on 8 May 2009. Central to this study is the comparison of the 8 May 2009 derecho environment to that of other mesoscale convective systems (MCSs) that occurred in the central United States during a similar time of year. Synoptic-scale forcing was weak and thermodynamic instability was limited during the development of the initial convection, but several mesoscale features of the environment appeared to contribute to initiation and upscale growth, including a mountain wave, a midlevel jet streak, a weak midlevel vorticity maximum, a ''Denver cyclone,'' and a region of upper-tropospheric inertial instability.

The subsequent MCS developed in an environment with an unusually strong and deep low-level jet (LLJ), which transported exceptionally high amounts of low-level moisture northward very rapidly, destabilized the lower troposphere, and enhanced frontogenetical circulations that appeared to aid convective development. The thermodynamic environment ahead of the developing MCS contained unusually high precipitable water (PW) and very large midtropospheric lapse rates, compared to other central plains MCSs. Values of downdraft convective available potential energy (DCAPE), mean winds, and 0–6-km vertical wind shear were not as anomalously large as the PW, lapse rates, and LLJ. In fact, the DCAPE values were lower than the mean values in the comparison dataset. These results suggest that the factors contributing to *updraft* strength over a relatively confined area played a significant role in generating the strong outflow winds at the surface, by providing a large volume of hydrometeors to drive the downdrafts.

1. Introduction

This study investigates the development of an intense derecho (Johns and Hirt 1987) that occurred on 8 May 2009 over the central United States (Fig. 1a). Homes and businesses were damaged, and trees and utility poles were downed over widespread regions from western Kansas to eastern Kentucky resulting from multiple wind gusts greater than 35 m s^{-1} and isolated gusts greater than 45 m s^{-1} (Fig. 1b). The associated mesoscale convective system (MCS; Zipser 1982) contained bow echoes (Fujita 1978) during a portion of its lifetime and an intense, long-lived mesoscale convective vortex (MCV; Davis and Trier 2007) developed during the latter stage of the MCS that was associated with very severe surface winds and tornadoes (Fig. 1). In addition, multiple tornadoes and localized swaths of intense wind damage occurred in association with strong meso-γ-scale (Orlanski 1975) vortices (Atkins and St. Laurent 2009) along the convective line, as seen in some extreme damaging-wind MCSs (Miller and Johns 2000; Wheatley et al. 2006).

Derechos have been observed during all months of the year and in most locales east of the Rocky Mountains but

Corresponding author address: Dr. Michael C. Coniglio, National Severe Storms Laboratory, Rm. 2234, National Weather Center, 120 David L. Boren Blvd., Norman, OK 73072.
E-mail: michael.coniglio@noaa.gov

DOI: 10.1175/2010MWR3413.1

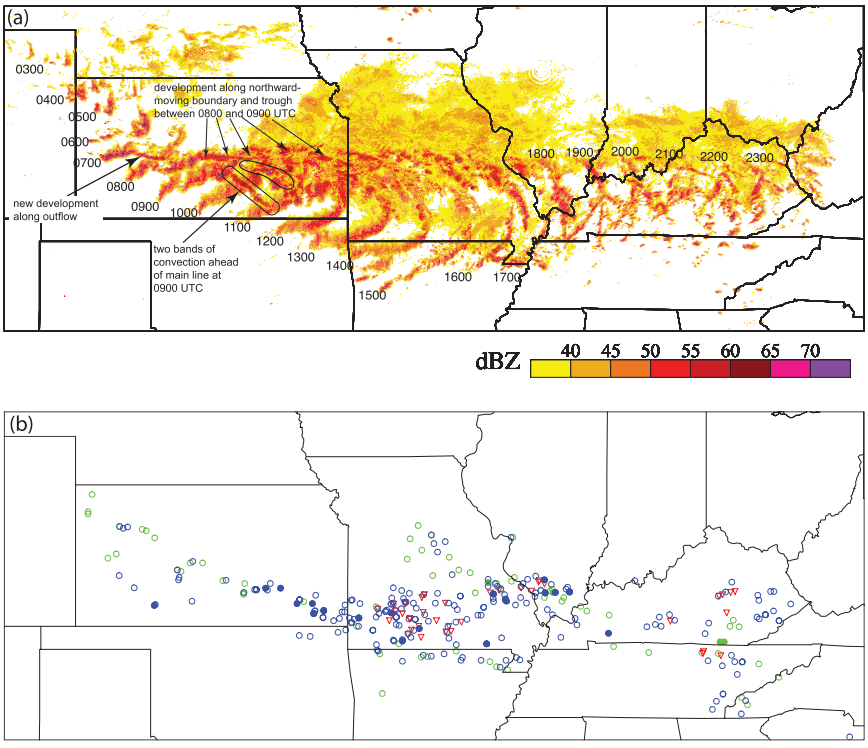

FIG. 1. (a) Hourly composite reflectivity images from the NMQ project plotted at 1-h intervals and (b) severe weather reports associated with the derecho-producing MCS [hail ≥0.75 in. (open green circles), hail ≥2.0 in. (filled green circles), wind damage or wind gusts ≥26 m s^{-1} (50 kt; open blue circles), wind gusts measured or estimated ≥33.5 m s^{-1} (65 kt; filled blue circles), and tornado reports (red)], from 0300 to 2300 UTC 8 May 2009.

occur most frequently in late spring and summer across the midwestern United States (Johns and Hirt 1987; Bentley and Sparks 2003; Coniglio and Stensrud 2004). The 8 May 2009 system developed in a way that is common for MCSs: convective initiation occurs along the eastern slopes of the Rocky Mountains and storms move eastward and consolidate in regions of lower-tropospheric warm advection, convergence, and conditional instability, all of which are enhanced by a nocturnal low-level jet (LLJ) (Blackadar 1957; Bonner 1968; McNider and Pielke 1981; Cotton et al. 1989; Laing and Fritsch 2000; Tuttle and Davis 2006). The development of a large, intense MCS resulted from a complex series of processes and mergers of several convective lines and clusters over a relatively short time period, which is also common for warm season MCSs (McAnelly et al. 1997; Jirak and Cotton 2003).

Along with the usual desire to study extraordinary weather phenomena, motivation for this study came from the issuance of a particularly dangerous situation (PDS) severe thunderstorm watch by the Storm Prediction Center (SPC) in the region of interest several hours prior to the first significant wind damage report (a graphic of the counties included in the severe thunderstorm watch and the associated text can be found at http://www.spc.noaa.gov/products/watch/2009/ww0264.html.)[1] This was one of only 19 PDS severe thunderstorm watches that were issued from 2002 to 2009 (G. Carbin, SPC, 2010, personal communication). The rarity of PDS severe thunderstorm watches and the long lead time of the watch are indications that there were signals in the precursor environment that a significant event was possible. However, as will be shown later, the environment of the 8 May 2009 derecho was not ''synoptically evident'' in that the convection was not forced by a synoptic-scale weather system with easily identifiable boundaries and forcing mechanisms.

The extremity of the event and the ability of the human forecasters to anticipate a particularly severe event prior to the development of the MCS compel one to ask the question, what, if anything, was unusual about the

[1] The second author of this paper was the lead forecaster on duty.

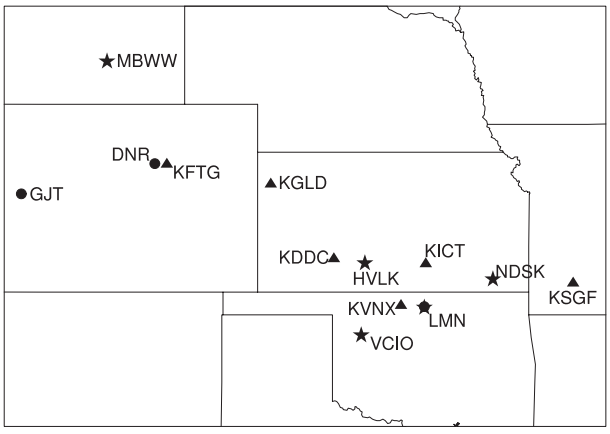

FIG. 2. Locations and names of the 915-MHz wind profiler sites (star), WSR-88D sites (triangle), and radiosonde sites (dot) used in this study.

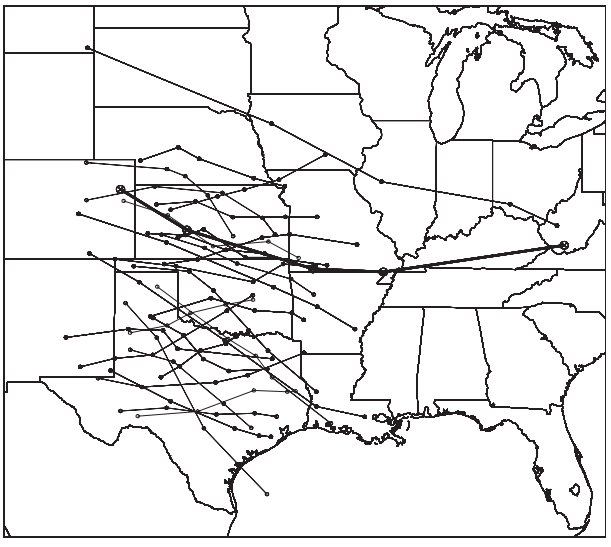

FIG. 3. Paths of the 28 MCSs (thin lines) from C2010 used in the comparison to the 8 May 2009 MCS (thick line). The points along the lines denote the locations of the first storms, genesis, mature, decay, and dissipation stages of the MCSs, respectively (see text for details).

environment? This question is addressed in this study by documenting the development of the MCS and its environment using routine observations and Rapid Update Cycle (RUC) analyses (Benjamin et al. 2004), then comparing these analyses to those of other MCSs that occurred over a similar location and time of the year. It will be shown that parameters typically associated with strong convective surface winds, like downdraft convective available potential energy (DCAPE), the surface-to-midtropospheric shear, and mean wind perpendicular to the convective line, were sufficient for the development of cold pools and organized severe thunderstorms but were not extraordinarily large compared to those found in the environments of other central plains MCSs. Rather, the environmental features that were highly anomalous were the midlevel lapse rates, moisture, and the LLJ.

Along with documenting the unusual aspects of the environment, another goal of this study is to document the complexity of the development and evolution of the convective event. Although the genesis and evolution of the MCV is a significant part of this event, the focus here is on the complex initiation and evolution of the convective system and its environment prior to the development of the MCV. We will focus on the system's early evolution since it is likely that the ability to accurately predict convective systems of this type is strongly related to a detailed understanding of the processes and environmental ingredients that can create such a system.

2. Data and methodology

The analysis of the 8 May 2009 convective system made use of radar data from the National Weather Service Weather Surveillance Radar-1988 Doppler (WSR-88D) network. This analysis included level II data from individual WSR-88D sites obtained from the National Climatic Data Center, base reflectivity composites generated by Unisys, and the composite (column maximum) reflectivity derived from the National Mosaic and Multisensor Quantitative Precipitation Estimation (NMQ) Project (Vasiloff et al. 2007). In addition, this study used surface and upper-air observations from a variety of platforms that were quality controlled by the National Oceanic and Atmospheric Administration (NOAA) Meteorological Assimilation Data Ingest System (MADIS) (see Fig. 2 for site locations of the radiosonde, wind profiler, and WSR-88D data used in this study). These data were used to document the complex development and early evolution of the convective event.

The MCS environment is examined further using the hourly RUC model analyses provided on a 20-km grid and on constant pressure surfaces spaced 25 hPa apart. To address the question of what was unusual about the environment, the RUC analysis of the 8 May 2009 event is compared to those from 28 MCSs obtained from the dataset described in Coniglio et al. (2010, hereafter C2010). This comparison dataset includes MCSs that occurred from early May to early June in the central United States (Fig. 3) and that had a nearly contiguous reflectivity region of 35 dBZ or more at least 100 km in length and embedded echoes of 50 dBZ or more for at least five continuous hours. Although not all of the comparison MCSs produced derechos or severe weather, all of them eventually transitioned into a leading line–trailing stratiform structure (Houze et al. 1989; Parker and Johnson

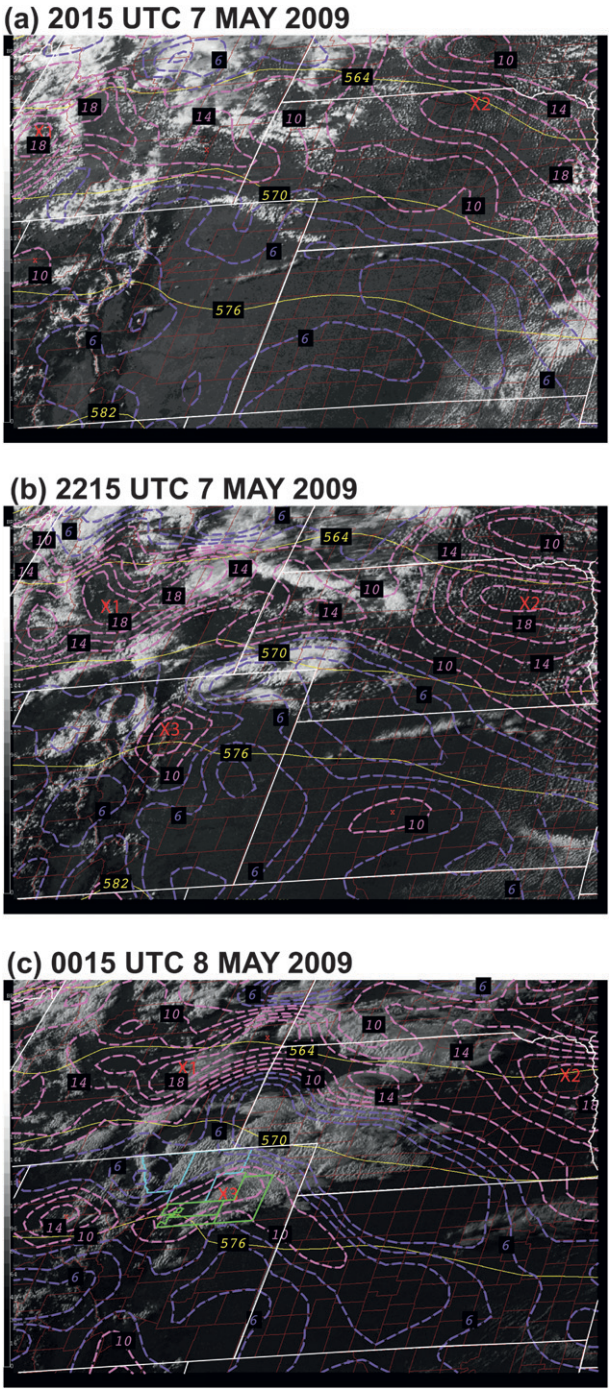

FIG. 4. Geostationary Operational Environmental Satellite (GOES) visible imagery for (a) 2015 UTC 7 May, (b) 2215 UTC 7 May, and (c) 0015 UTC 8 May. Also displayed are the RUC analyses of 500-hPa geopotential heights (dam; yellow) and 500-hPa absolute vorticity (every 10^5 s^{-1}; dashed purple and magenta lines). The weak vorticity maxima over WY and NE discussed in the text are indicated by X1 and X2, respectively. The weak vorticity maximum over central CO is indicated in (b) and (c) by X3. Weld and Larimer Counties, CO, are outlined in light blue and Adams, Arapahoe, Washington, and Morgan Counties, CO, are outlined in green.

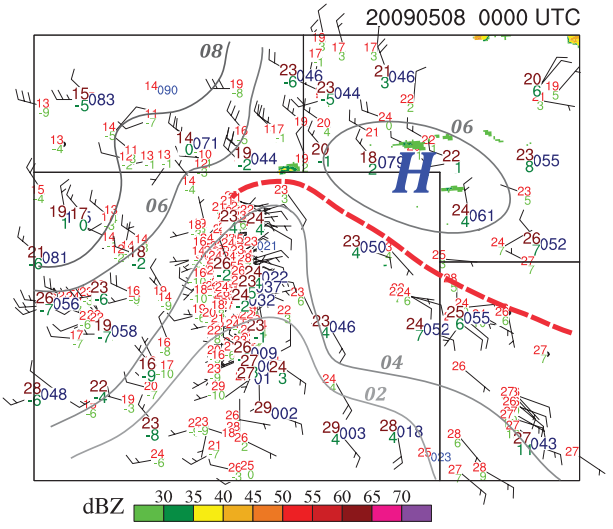

FIG. 5. Manual surface analysis valid 0000 UTC 8 May. Sea level pressure (gray solid lines) is analyzed every 2 hPa. The observations include 2-m temperature (°C; red), 2-m dewpoint (°C; green), sea level pressure (hPa; blue), and winds (full barb every 5 m s^{-1}). The dashed red line indicates a trough–wind shift line. The darker colors and larger font depict aviation routine weather report (METAR) observations and the lighter colors and smaller font depict observations from various mesoscale observation networks. Also included is the NMQ composite reflectivity mosaic.

2000) that resembled the mature structure of the 8 May 2009 MCS.

In the C2010 study, changes in the environment relative to the location and movement of the MCSs are examined by producing composite RUC analyses at several stages in the MCS life cycle, including the pre-deep-convective environment (termed the first storms stage in C2010) and the environment ahead of newly developed MCSs (termed the genesis stage in C2010). The environment at the time of the first storms and genesis stages of the 8 May 2009 MCS will be compared to the composite environments of the first storms and genesis stages for the 28 other MCSs in the C2010 dataset using standardized anomalies a_s, where $a_s = (x_a - \overline{x})/\sigma_x$ is calculated at each grid point, x_a is a gridpoint value of a variable x in the RUC analysis for the 8 May 2009 event, $\overline{x}$ is the mean of x from the C2010 MCS dataset, and σ_x is the sample standard deviation of x from the C2010 MCS dataset. The first storms and genesis stages of the 8 May 2009 MCS are defined to be at 0300 and 0700 UTC, respectively. Examination of the anomalies in this manner allows an investigation of what was unusual about the environment of the 8 May 2009 derecho compared to other MCS environments that occurred in a similar place and time of the year.

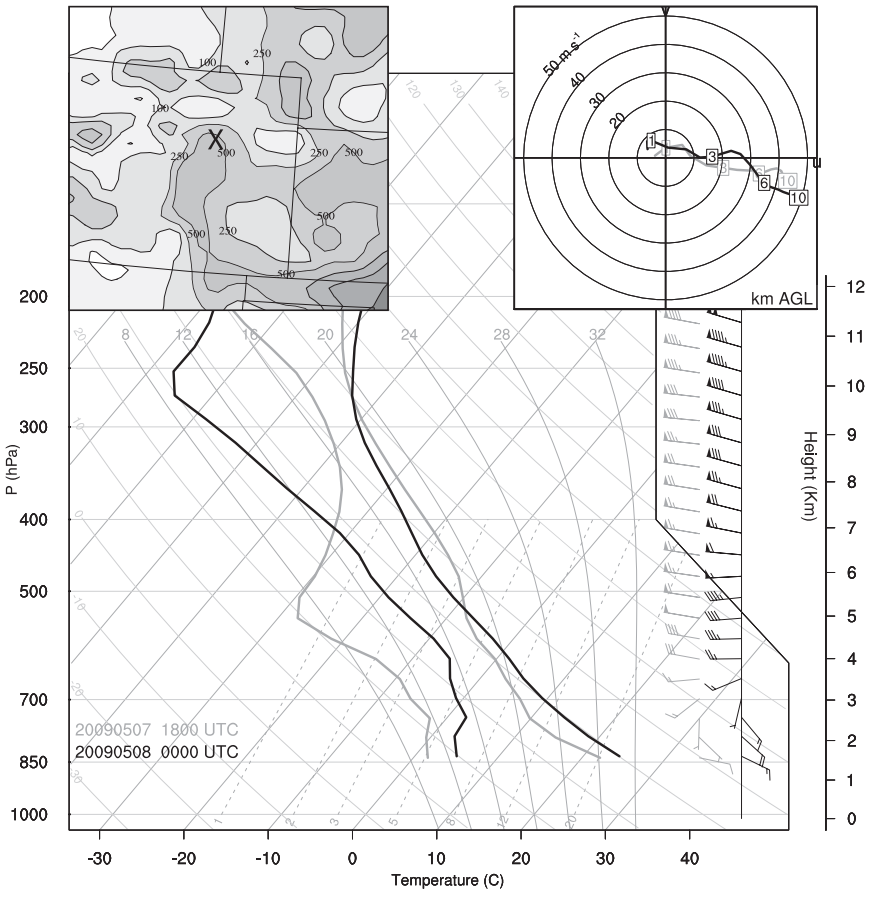

FIG. 6. Skew *T* diagram of temperature and dewpoint and hodograph (upper right inset) valid 1800 UTC 7 May 2009 (light gray lines and winds) and 0000 UTC 8 May 2009 (black lines and winds) from the RUC analysis at the location in northeastern CO marked with × in the upper-left inset. Half (full) barbs are drawn every 2.5 (5) m s^{-1} and pennants are drawn at 25 m s^{-1}. The inset in the upper left also shows the RUC analysis of MUCAPE (contours of 10, 100, 250, 500, and every 500 m^2 s^{-2} thereafter) valid 0000 UTC 8 May.

3. Analysis

a. Environmental conditions preceding deep convective development

Relatively dry conditions and few clouds covered much of the central high plains in the early afternoon of 7 May (Fig. 4a). A band of cumulus developed over far northeastern Colorado (Fig. 4a) near the western end of a surface trough (Fig. 5) that extended from a weak cyclone over far eastern Nebraska. Cloud bases were relatively high, atop a boundary layer that was moistening with time but remained relatively dry through 0000 UTC (Fig. 6). Nearby WSR-88Ds detected light precipitation, mostly less than 35 dB*Z*, with this initial cloudiness (Fig. 5), much of which did not appear to reach the ground. The limited CAPE in this region (Fig. 6) likely limited the strength of any convection initially.

Vertical motion and potential temperature fields in vertical cross sections (Fig. 7) suggest that mountain waves were partially responsible for the initial clouds and precipitation. Upstream conditions in which strong mountain waves are likely to develop are evident in the nearby RUC sounding (Fig. 6) and in the nearby 0000 UTC observed soundings (not shown). These conditions consist of (i) strong wind at mountaintop level, increasing with height and oriented perpendicular to the mountain range throughout a deep layer, and (ii) a relatively stable layer near mountaintop height with weaker stability at higher levels (Durran 1986). Furthermore, a persistent local maximum in low-level westerly flow over the terrain in far southern Wyoming (Fig. 5) appears to enhance the convergence and upward motion locally over far southeastern Wyoming, before the shallow convection first appears.

The northeastern Colorado–southeastern Wyoming–Nebraska border region was also under the right-entrance

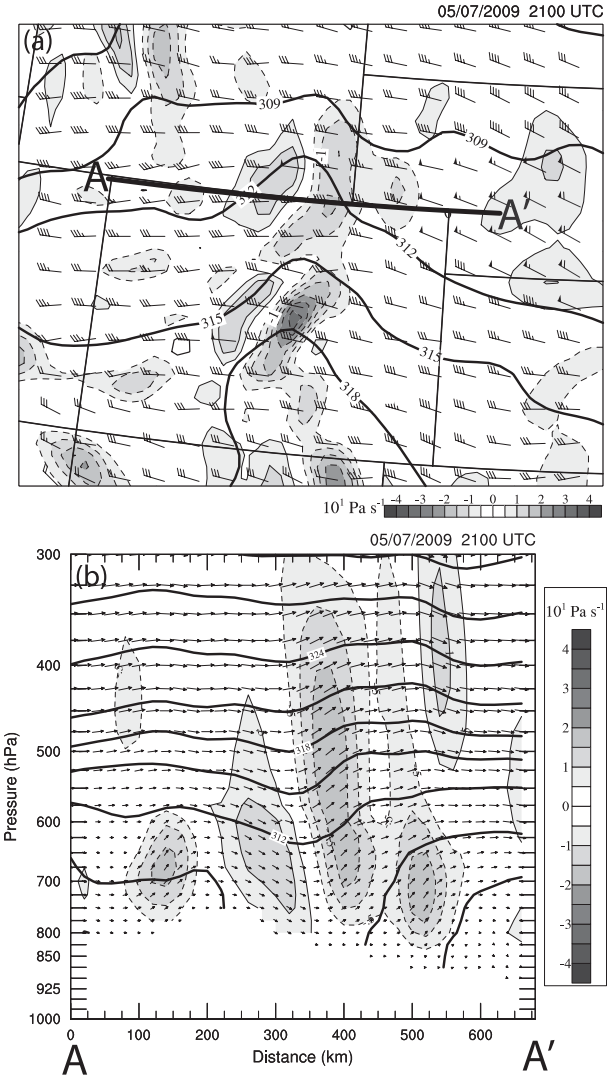

FIG. 7. (a) RUC analysis of 600-hPa pressure vertical velocity contoured and shaded every 0.5×10^1 Pa s^{-1} (negative values dashed) and potential temperature contours in thick black lines every 3 K valid 2100 UTC 7 May 2009. Half (full) wind barbs are drawn every 2.5 (5) m s^{-1} and pennants represent 25 m s^{-1}. (b) As in (a), but for a vertical cross section along the line shown in (a) and with vectors illustrating the flow in the plane of the cross section.

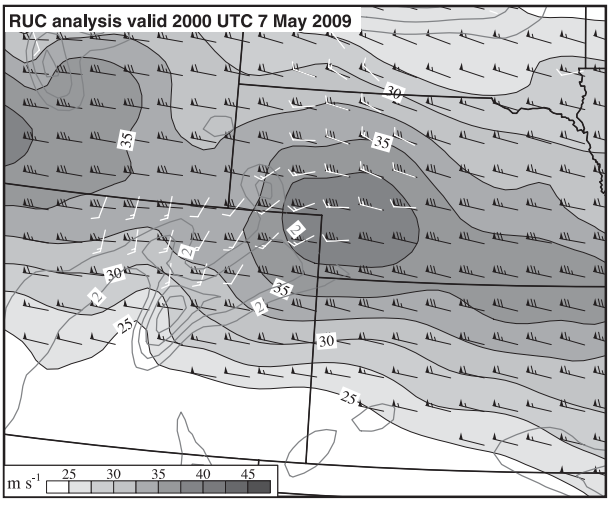

FIG. 8. RUC analysis of 450-hPa total wind, ageostrophic wind, and horizontal divergence valid at 2000 UTC 7 May 2009. Total wind speed is shaded every 2.5 m s^{-1} starting at 25 m s^{-1} and is represented by the black wind barbs. The white wind barbs represent the ageostrophic wind. Full wind barbs are drawn every 5 m s^{-1} and pennants represent 25 m s^{-1}. Horizontal divergence is contoured every 2×10^5 s^{-1} starting at 2×10^5 s^{-1} (gray lines).

region of a midlevel jet streak (Fig. 8), which is often collocated with MCS development (Maddox 1983; Johns 1993; Coniglio et al. 2004). The flow is significantly ageostrophic in this region (Fig. 8), which may be the result of the jet-streak dynamics (Uccellini and Johnson 1979) and the leeside flow deceleration associated with terrain-induced waves (Durran 1986). Furthermore, upslope flow and an associated "Denver cyclone" (Szoke et al. 1984) were evident in the surface observations (Fig. 5) and in animations of WSR-88D level II data from the Denver, Colorado (KFTG, not shown), site. Coincident with the Denver cyclone was the development of a weak midlevel vorticity maximum over the heated terrain of the Rockies in north-central Colorado (Figs. 4b and 4c). Finally, the southern fringe of a midlevel shortwave trough traversing Wyoming approached the area and may have contributed to the lift by 0000 UTC (Fig. 4c). All of these factors likely contributed to the upward vertical motion and subsequent weak convective development in eastern Colorado and far southeastern Wyoming by 0000 UTC.

After 0000 UTC, weak convection continued to develop over northern Weld and eastern Larimer Counties in Colorado (highlighted in light blue in Fig. 4c). A southwestward-moving outflow boundary originating from this convection and evident in WSR-88D imagery (not shown) appeared to help initiate convection over Adams, Arapahoe, Washington, and Morgan Counties (highlighted in light green in Fig. 4c). Precipitation falling through the deep, well-mixed boundary layer with very steep low-level lapse rates (Fig. 6) likely fostered the development of evaporatively cooled air that expanded rapidly over northeastern Colorado through 0300 UTC (Fig. 9a).

b. Evolution of the environment and convection prior to MCS development

Much stronger convection developed shortly after 0300 UTC near the intersection of the outflow boundary and the preexisting pressure trough over southern Yuma

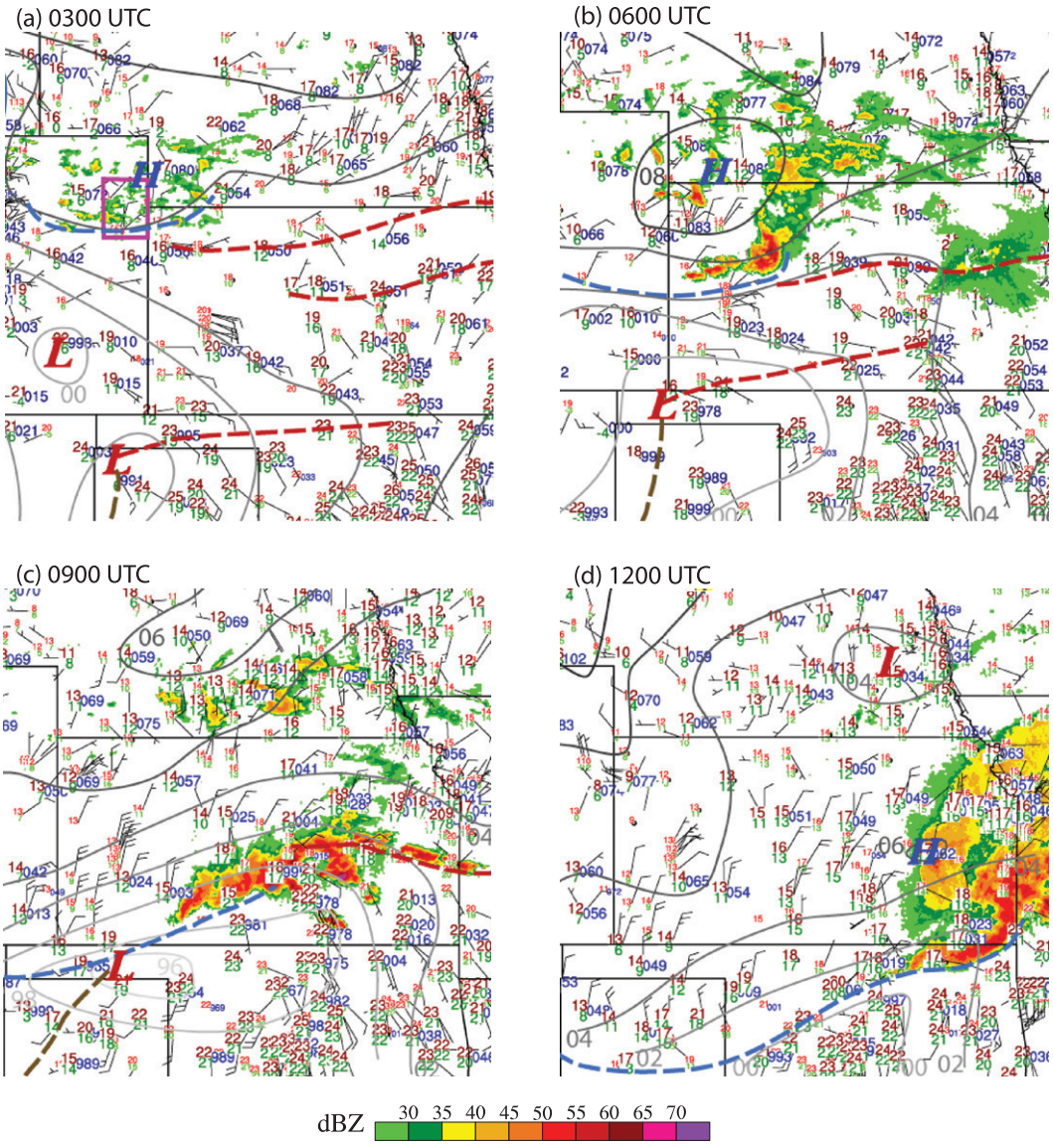

FIG. 9. Manual surface analyses valid every 3 h from (a) 0300 to (d) 1200 UTC 8 May. Sea level pressure (gray solid lines) is analyzed every 2 hPa. The observations include 2-m temperature (°C; red), 2-m dewpoint (°C; green), sea level pressure (hPa; blue), and winds (full barb every 5 m s^{-1}). Dashed red lines indicate troughs–wind shift lines and the dashed blue lines indicate the convective outflow boundary. The darker colors and larger font depict METAR observations and the lighter colors and smaller font depict observations from various mesoscale observation networks. Also included is the NMQ composite reflectivity mosaic.

County in northeastern Colorado (outlined in purple in Fig. 9a). Although the convection was deeper, it likely continued to be high based, as RUC analyses in this region showed lifting condensation levels generally over 2000 m AGL (Fig. 6). Furthermore, it is noteworthy that the instability at this stage of MCS development is very low compared to the environments just prior to deep convective initiation for the 28 MCSs in the C2010 dataset (Fig. 10). The largest values of most unstable convective available potential energy (MUCAPE) were only 300 m^2 s^{-2} ahead of the first storms over far eastern Colorado and northwestern Kansas (Fig. 10a). These values are more than two standard deviations below the mean MUCAPE for the 28 MCSs in the comparison dataset (Fig. 10d). The low MUCAPE resulted from the lack of boundary layer moisture and relatively small midlevel lapse rates (Fig. 6).

The reasons why the convection intensified after 0300 UTC are not obvious, but there is evidence that the localized environmental conditions were rapidly becoming more favorable for stronger convection. For example, the

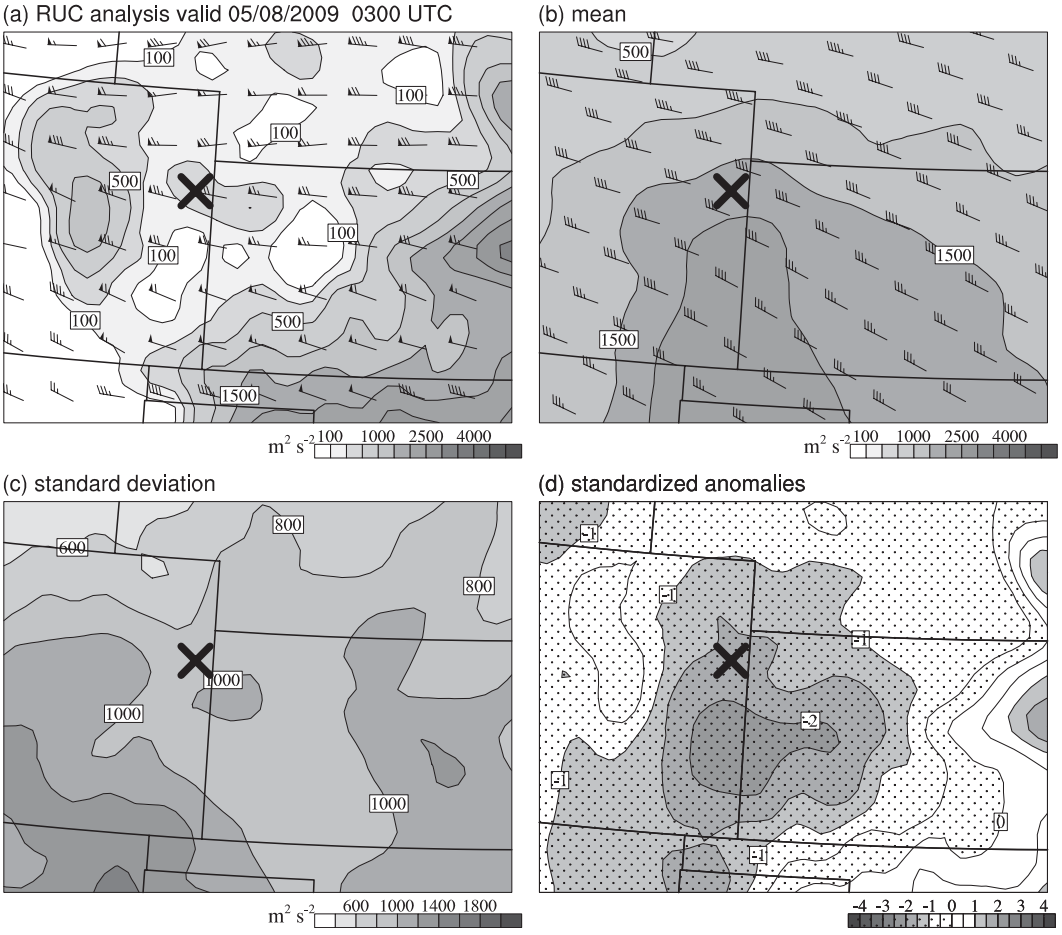

FIG. 10. (a) RUC analysis of MUCAPE shaded and contoured with values of 100, 250, and 500 $m^2\ s^{-2}$, then every 500 $m^2\ s^{-2}$ thereafter, and 0–6-km wind shear vectors (full barb = 5 m s^{-1}, pennant = 25 m s^{-1}). The × marks the location of the strong convective development shortly after 0300 UTC. (b) As in (a), but for the mean MUCAPE ahead of the first storms of developing MCSs from the set of 28 MCSs described in section 3, where × marks the location of ensuing first storms development that was used in the compositing procedure. (c) As in (b), but for the standard deviation of MUCAPE from the set of 28 MCSs shaded and contoured every 200 $m^2\ s^{-2}$, and (d) MUCAPE standardized anomalies based on a comparison to the C2010 dataset, with the negative anomalies hatched.

RUC analysis indicated an increase in horizontal convergence associated with the strengthening cold pool and strengthening southerly flow of higher equivalent potential temperature θ_e air aloft in the 1–2-km AGL layer prior to the convective development (not shown). Furthermore, the dry subcloud air (Fig. 6) facilitated rapid organization of cold pools and was one of the factors recognized by the SPC forecasters that indicated the potential for cold pool consolidation and MCS development. Indeed, the stronger thunderstorms that developed after 0300 UTC persisted and moved east-southeast into northwestern Kansas. Despite the limited instability, the strong westerly flow aloft created substantial 0–6-km vertical wind shear (Fig. 10a) that favored organized thunderstorms along the downshear side of the cold pool that expanded south and east through 0600 UTC (Fig. 9b).

Furthermore, preceding deep-convective development, a large region of upper-tropospheric negative geostrophic potential vorticity PV_g was found over western Kansas (Fig. 11a), where the deep convection subsequently grew upscale. Negative PV_g is a necessary condition for inertial instability on isentropic surfaces in a dry, gravitationally stable atmosphere.[2] An atmosphere that is weakly stable

[2] The dry-air potential temperature was used in the static stability term of PV_g. We also used θ_e and θ_e^* (saturated equivalent potential temperature) in the stability calculation, as discussed in Schultz and Schumacher (1999), and the results were almost identical, likely because the PV_g is assessed in the upper troposphere, where the low absolute moisture content results in only slight differences in the three versions of potential temperature.

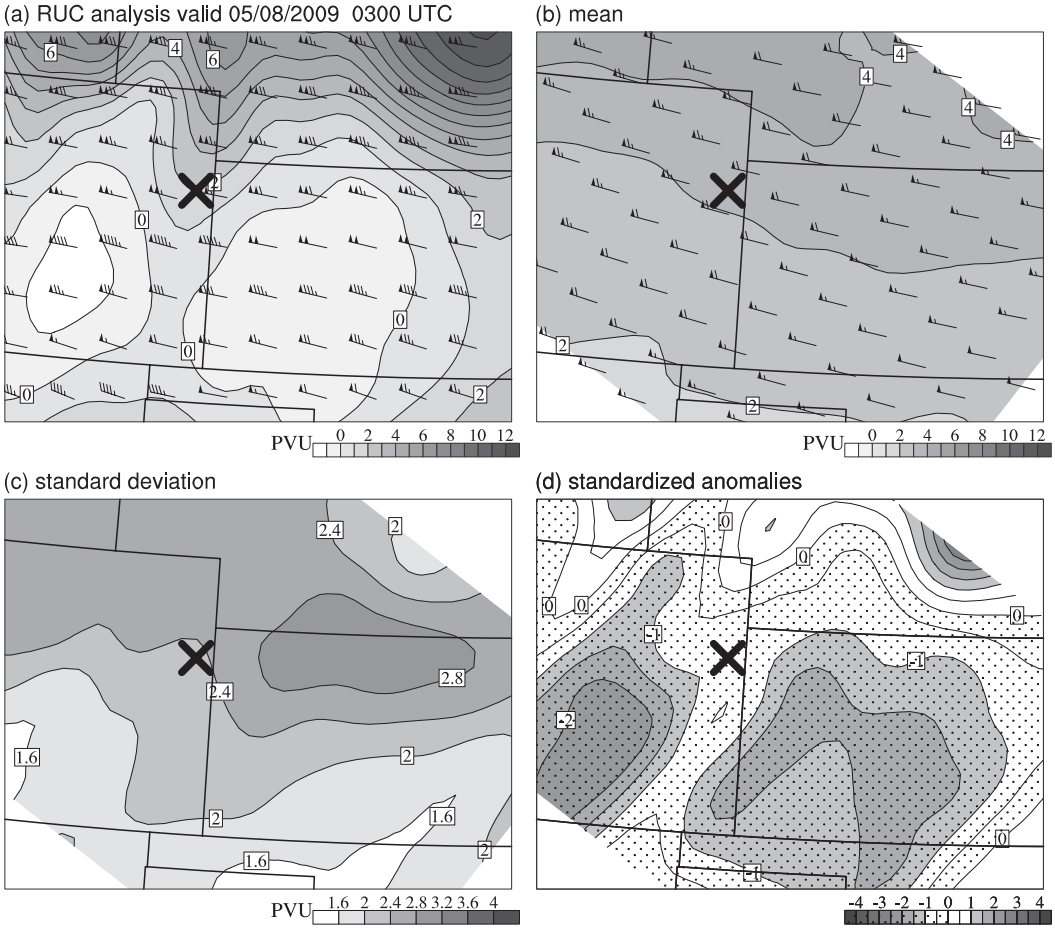

FIG. 11. As in Fig. 8, but for geostrophic potential vorticity and geostrophic winds (full barb = 5 m s^{-1}, pennant = 25 m s^{-1}) on the 345-K potential temperature surface (1 PVU = 10^{-6} m^2 s^{-1} K kg^{-1}).

(or unstable) inertially favors the efficient ventilation of convective outflow in the upper troposphere (Emanuel 1979; Seman 1994) and low values of PV_g may signal the rapid upscale growth of MCSs (Blanchard et al. 1998; Schultz and Knox 2007; C2010). Not only were the values of PV_g low in an absolute sense, but they were also low compared to the environments of other MCSs, with standardized anomalies in the −1.5 to −2 range (Fig. 11d). As hypothesized in Seman (1994) and Blanchard et al. (1998), weak ambient inertial stability is important to the development of deep mesoscale circulations that can support additional convection on the baroclinically warm side of the circulation (usually equatorward in the Northern Hemisphere). Presumably in the 8 May 2009 case, the efficient ventilation of updraft mass in the weak ambient inertial instability may have compensated for the relative lack of conditional instability initially.

The atmosphere was undergoing rapid changes by 0600 UTC. A strong LLJ had developed and was tapping into a reservoir of very moist air over western Oklahoma and the Texas Panhandle. The low-level horizontal convergence (not shown) increased in the region ahead of the LLJ and south of the outflow boundary that extended west from the original convection (see Fig. 9b). Thunderstorms subsequently developed along this southward-surging outflow boundary in west-central Kansas at 0600 UTC (Fig. 9b). After 0600 UTC, convective outflow surged 20–30 km ahead of the weakening original convection, and explosive convection subsequently developed along the outflow boundary by 0700 UTC (Fig. 1a).

c. *Mature MCS evolution between 0600 and 1200 UTC*

The evolution of convection after 0600 UTC was quite complex and is documented next for the purpose of showing the departure it represents from the cleaner and simpler environments that are the focus of the MCS modeling literature. New thunderstorms developed along a northward-moving boundary that appeared to be associated with a pressure trough extending eastward from the

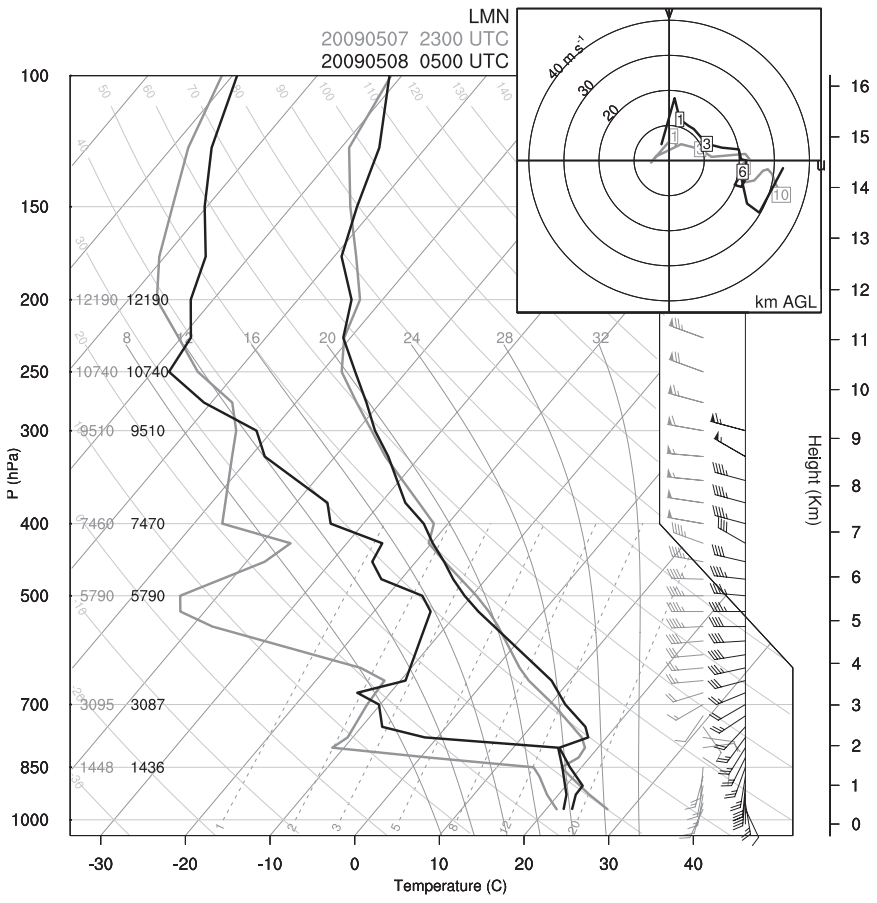

FIG. 12. Skew *T* diagrams and hodographs from observed soundings at LMN (see Fig. 2 for location) valid at 2300 UTC 7 May 2009 (gray lines) and 0500 UTC 8 May 2009 (black lines). Full wind barbs represent 5 m s^{-1} and pennants represent 25 m s^{-1}.

low pressure center over the Oklahoma–Texas Panhandles (Fig. 9a). This boundary also appeared to mark the steepest gradient in moisture from the moderately moist air mass over south-central Kansas and the very moist Gulf of Mexico air mass to the south, as seen in a comparison of soundings taken at 2300 UTC on 7 May and at 0500 UTC on 8 May at Lamont (LMN) in north-central Oklahoma (Fig. 12). Perhaps as a consequence of the rapidly strengthening and deepening low-level flow (seen in Fig. 12 and discussed in more detail in section 3d), the northward-moving boundary appeared to sharpen with time in the WSR-88D level II data from Wichita, Kansas (KICT), prior to the initiation of the convection along it. After 0800 UTC, this new line of convection merged with the main area of convection farther west (labeled band A in Fig. 13). Shortly thereafter, additional thunderstorms developed along the preexisting trough over east-central Kansas (identified in Fig. 9b), merged with the other areas of convection, and expanded eastward to the Kansas–Missouri border by 0900 UTC (the easternmost segment labeled D in Fig. 13).

Adding to the complexity of the convective development were two bands (labeled B and C in Fig. 13) that developed ahead of the main convective line after 0800 UTC. Examination of WSR-88D level II data revealed bands of local maxima and minima in clear-air reflectivity and systematic variations in radial velocity that were oriented perpendicular to the LLJ, which propagated to the northeast (not shown), perhaps marking the "nose" of the LLJ. One of the better-defined clear-air reflectivity bands appeared to mark the transition in 2-km AGL wind from 15 m s^{-1} at 0600 UTC to 25 m s^{-1} at 0700 UTC as the band passed the Haviland, Kansas (HVLK), profiler site (Fig. 14). Convective band B (Fig. 13) developed along this feature as it moved north and east. Likely aiding the convective development was the strong horizontal convergence and low-level deformation frontogenesis along the leading edge of the LLJ (Fig. 13). This conclusion is supported by the fact that bands B and C are aligned with the long axis of the frontogenesis (Fig. 13).

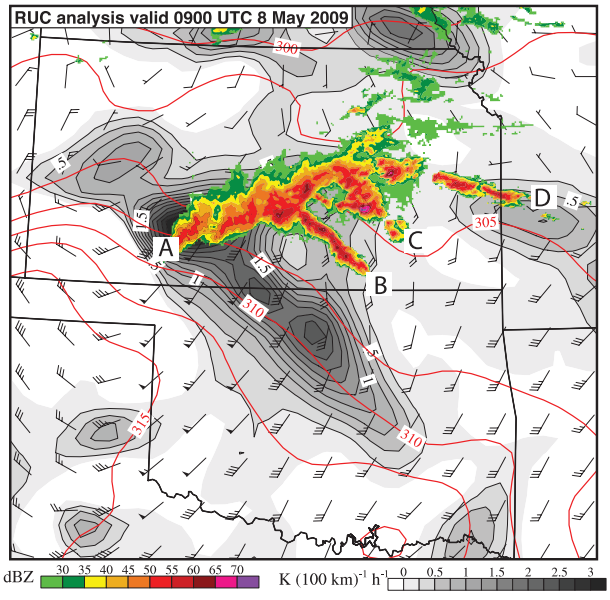

FIG. 13. RUC analysis of 2D frontogenesis shaded and contoured every 0.25 K (100 km)$^{-1}$ h^{-1}, wind vectors (full barb = 5 m s^{-1}, pennant = 25 m s^{-1}), and potential temperature (red contours every 2.5 K) on the 825-hPa surface valid 0900 UTC 8 May 2009, with the NMQ composite reflectivity overlaid.

By 0900 UTC, the western half of band A was changing orientation from nearly east–west to southwest–northeast with time (Fig. 13). At this time, band B was expanding and intensifying while band C was decreasing in coverage and intensity. The intersection of bands A and B formed a pivot point for the change in line orientation and marked the northern extent of a subsequent small-scale bow echo and an area of mesovortices that produced wind gusts over 36 m s^{-1} and significant property damage in the vicinity of KICT after 0900 UTC. The western half of the convective line developed a larger-scale bow echo and accelerated to the east-southeast as the system became oriented more perpendicular to the mean wind (Figs. 9c and 9d). This pattern of behavior is consistent with the idea that, as a cold pool consolidates, rapid downwind cell regeneration and propagation are favored along the portion of the outflow that becomes oriented perpendicular to a wind profile that is nearly unidirectional and contains shear over some depth of the troposphere (Weisman 1993; Corfidi 2003; Cohen et al. 2007), which could be a reflection of the importance of vertical momentum transport within the leading portions of the MCS cold pool (Mahoney et al. 2009).

After the development of the bow echo, numerous intense convective cells continued to develop in the vicinity of the intersection of bands A and B, where a very large area of nearly contiguous radar reflectivity echoes greater than 45 dBZ was concentrated over southeastern Kansas by 1000 UTC (Fig. 1a). Through 1200 UTC, the system accelerated and moved perpendicular to the mean deep-layer wind/shear and developed a larger-scale bow-echo structure as it entered southwest Missouri after 1200 UTC. Ahead of the storms, the slightly backed flow in the 0.5–1.5-km layer was unusually strong (Figs. 14 and 15) and allowed for very efficient storm-relative inflow of very unstable air that supported the continued regeneration of strong convection along the advancing cold pool (Fig. 9d).

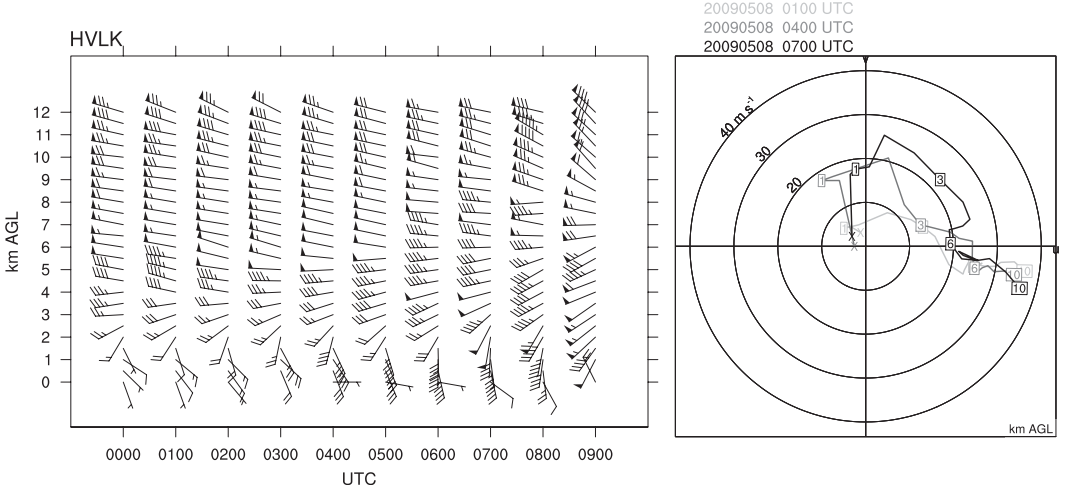

FIG. 14. Hourly wind profiles from HVLK from 0000 to 0900 UTC 8 May 2009. Full wind barbs represent 5 m s^{-1} and pennants represent 25 m s^{-1} and hodographs valid at 0100 (light gray line), 0400 (medium gray line), and 0700 UTC (black line). The 10-m wind from the nearest surface station was used for the surface wind. The MCS reached the HVLK site shortly after 0900 UTC.

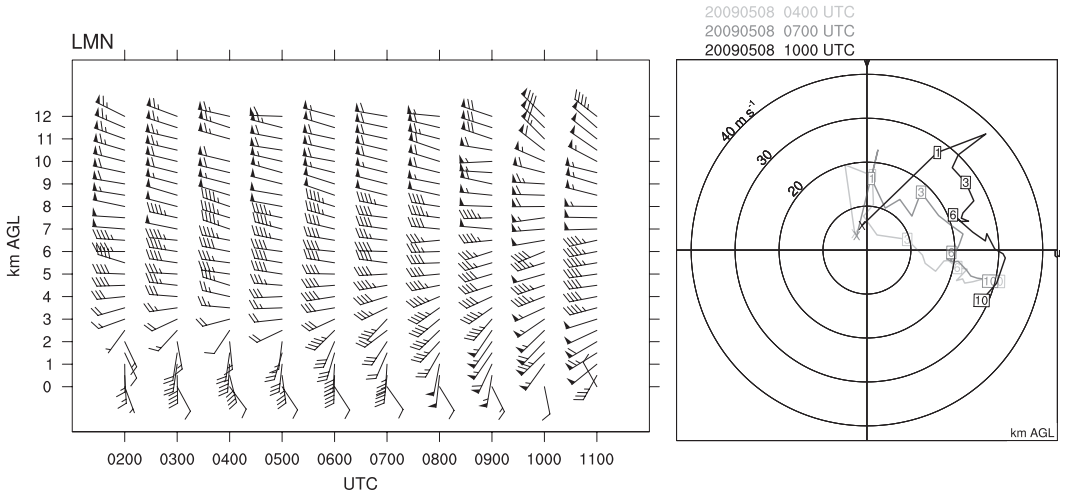

FIG. 15. Hourly wind profile from LMN from 0200 to 1100 UTC 8 May 2009. Full wind barbs represent 5 m s^{-1} and pennants represent 25 m s^{-1} and hodographs valid at 0400 (light gray line), 0700 (medium gray line), and 1000 UTC (black line). The 10-m wind from the nearest surface station was used for the surface wind.

d. Evolution of the LLJ

One of the remarkable characteristics of the environment of the 8 May 2009 derecho was that the LLJ was both unusually strong and also very deep. The weak winds at 2300 UTC in the 900–800-hPa layer at LMN were replaced with stronger southerly and southwesterly winds by 0500 UTC (Fig. 12). A deepening of the LLJ also is seen in the wind profile at HVLK (Fig. 14) and is particularly evident at LMN, where the west-southwest wind at 3 km AGL increased from 10 m s^{-1} at 0400 UTC to 28 m s^{-1} out of the southwest at 1000 UTC (Fig. 15). The low-level wind speeds were measured as high as 38 m s^{-1} at 1000 UTC (at 1.5 km in Fig. 15), which further emphasizes the unusual strength of the LLJ for this event.

The Blackadar (1957) decoupling mechanism for LLJ formation usually confines the stronger wind speeds to near the top of the nocturnal boundary layer (McNider and Pielke 1981), which appeared to be below 1 km AGL (Fig. 12), so the explanation for this unusually deep LLJ likely lies elsewhere. The very deep LLJ could be related to (i) the coupling of the low-level southerly ageostrophic flow to the midlevel ageostrophic circulation and jet streak (Uccellini and Johnson 1979) that was moving across the area (Fig. 7), (ii) the ageostrophic circulation associated with a band of frontogenesis crossing the region (Fig. 11), or (iii) the strengthening of the lee trough over the Texas–Oklahoma Panhandles (Fig. 5). Regardless of the mechanism, the result was a deep mesoscale surge of strong low-level inflow winds into south-central Kansas toward the developing convective system.

In addition to its unusual strength and depth, the LLJ was also very extensive. At 0700 UTC, the time of MCS genesis, wind speeds at 500 m AGL were greater than 30 m s^{-1} in the wind profile at Vici, Oklahoma (VCIO; not shown), and were analyzed to be greater than 25 m s^{-1} over much of the western part of the state (Fig. 16a). Furthermore, 500-m AGL wind speeds >20 m s^{-1} covered much of Oklahoma and the Texas Panhandle, resulting in a large area of $a_s > 2$ over most of Oklahoma and peak values of $a_s > 3$ in some locations in the jet core (Fig. 16d). A strong and broad LLJ was anticipated by the short-term numerical forecast guidance (not shown) (although not as strong or broad as revealed by observations and analyses), and this guidance played a role in the issuance of the PDS watch.

e. Evolution of the thermodynamic environment after MCS development

Along with the strong surge of southerly flow, the environment ahead of and feeding into the developing MCS by 0700 UTC became very moist. In fact, a sizeable region of precipitable water (PW) over 5 cm is analyzed over southern Kansas (Fig. 17a), in which $a_s > 3$ in some areas (Fig. 17d). The standardized anomalies are large in the region where the MCS developed bow-echo characteristics and accelerated to the east-southeast (Fig. 9d). Very high low-level moisture content is a common characteristic of severe, long-lived MCSs in both the warm and cool seasons (Johns and Hirt 1987; Johns 1993; Coniglio et al. 2004; Burke and Schultz 2004).

Also in contrast to the environment for the initial convective development was a region of very large midlevel

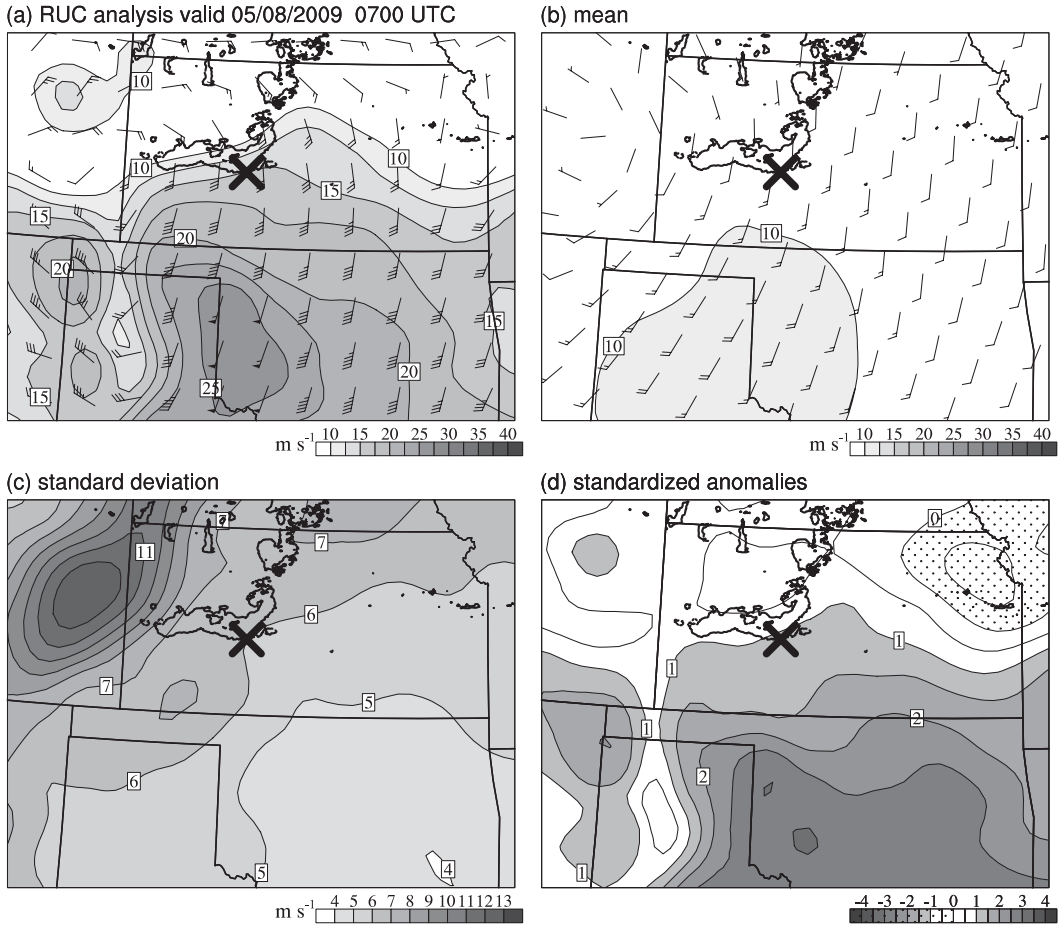

FIG. 16. (a) RUC analysis of 500-m AGL wind speed shaded and contoured every 2.5 m s^{-1}, starting at 10 m s^{-1} (full barb = 5 m s^{-1}, pennant = 25 m s^{-1}) valid at 0700 UTC 8 May 2009. The × marks a location near the center of the leading convective line that was used for the comparison of the analysis to the C2010 dataset. (b) As in (a), but for the mean 500-m AGL wind speed ahead of the newly developed MCSs from the set of 28 MCSs described in section 3, where × marks the location near the center of the leading convective line that was used in the compositing procedure. (c) As in (b), but for the standard deviation of 500-m AGL wind speed from the set of 28 MCSs shaded and contoured every 1 m s^{-1}, and (d) 500-m AGL wind speed standardized anomalies based on a comparison to the C2010 dataset, with the negative anomalies hatched.

lapse rates (3–6-km lapse rates greater than 8.5 K km^{-1}) ahead of the maturing MCS (Fig. 18a). In fact, the values of $a_s > 4$ for the lapse rates in far north-central Oklahoma (Fig. 18d) were the largest standardized anomalies found for any variable at any time during the MCS development. Consequently, the very steep lapse rates and the high moisture content in the lowest 2 km AGL (Fig. 12) produced unusually large values of CAPE along the ensuing MCS path, particularly in the few kilometers above the level of free convection.

Recall that our motivation to study this event arose from the ability of the SPC to anticipate an unusually strong convective wind event. The recognition of sufficient (although not unusually large) downdraft CAPE (DCAPE) to help organize convective outflows early in the convective event and sufficient mean flow/deep shear to organize the convective updrafts played a role in the decision-making process. But the recognition of very high PW values and lapse rates in the downstream environment played a decisive role in the decision to issue a PDS severe thunderstorm watch for this event, along with the recognition that a strong LLJ impinging on this area was likely to lead to an abundance of strong thunderstorms in a relatively confined region. A high spatial concentration of thunderstorms commonly precedes derechos, as perceived by the second author based on his operational experience.

Another interesting difference between the environment of the initial stages of the convection, and that ahead of the developing MCS, is the change in evaporative potential for convective downdrafts. Although the evaporation potential

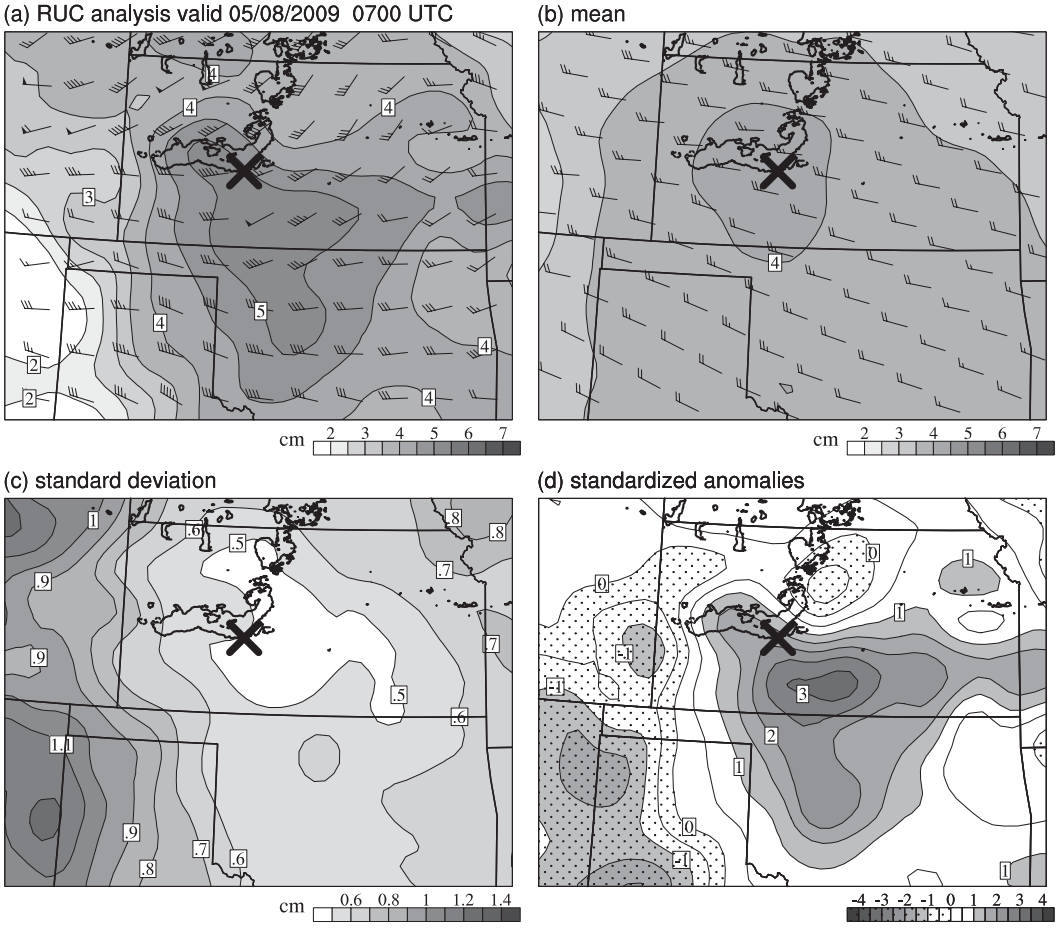

FIG. 17. As in Fig. 16, but for the PW (shaded and contoured every 0.5 cm) and 0–3-km wind shear vectors (full barb = 5 m s^{-1}, pennant = 25 m s^{-1}) valid at 0700 UTC 8 May 2009.

was sizeable during the pre-MCS stage of the event (prior to 0600 UTC) because of the dry, well-mixed boundary layer (Fig. 6), the DCAPE[3] values in the immediate downshear environment after the development of the MCS were generally less than the typical DCAPE values for other MCS environments (Fig. 19). Although substantial dryness was found in midlevels at 0500 UTC (Fig. 12), the relatively small lapse rates in the very moist surface-to- 800-hPa layer, and the continued moistening of the midlevel environment throughout the evening, limited the magnitude of the DCAPE of the presumed downdraft parcels. Accordingly, available observations reveal the lack of a strong cold pool at the surface through 1200 UTC. Surface temperatures generally fell only 4–6 K after the passage of the convective line during its intense stages between 0900 and 1200 UTC (Figs. 9c and 9d). Surface temperature deficits were commonly much larger for the MCSs studied by Engerer et al. (2008) (likely because several daytime cases were included in their dataset), but the temperature deficits of 4–6 K were similar to those found for the nocturnal bow echoes examined in Adams-Selin and Johnson (2010).

The finding of relatively small DCAPE and the lack of a strong cold pool at the surface strengthens one of the key arguments of this analysis; the unusually high PW content and midlevel lapse rates suggest a primary role of the updraft strength, in the ensuing development of the strong outflows. Given the modest evaporative cooling potential in the early mature stages of the MCS, and the abundant storm development in a relatively confined region over southeastern Kansas between 1000 and 1100 UTC (Fig. 1a), it is hypothesized that the melting and/or loading of the large volume of precipitation generated by these abundant, strong updrafts

[3] DCAPE was calculated in two ways in this analysis: 1) by using the parcel with the thermodynamic properties of the wet-bulb zero height and 2) by using the parcel with the minimum equivalent wet-bulb potential temperature up to 500 hPa. The results for the former are illustrated in the figures.

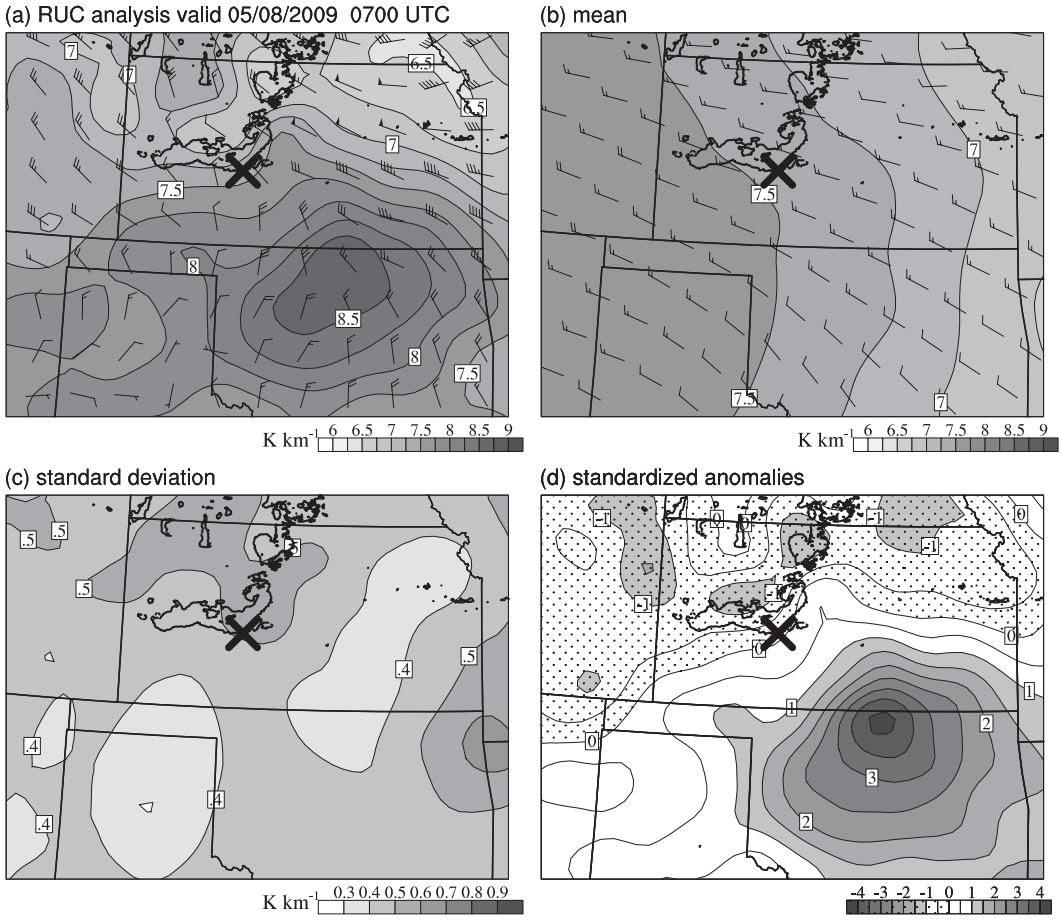

FIG. 18. As in Fig. 16, but for the 3–6-km lapse rates (shaded and contoured every 0.25 K km^{-1}) and 3–6-km wind shear vectors (full barb = 5 m s^{-1}, pennant = 25 m s^{-1}) valid at 0700 UTC 8 May 2009.

played a proportionally very large role in driving large downdraft mass fluxes and resulting strong outflows and severe surface winds. Downdrafts are dependent on updrafts for the hydrometeors that drive them, through diabatic effects as well as precipitation drag (water loading). Thus, in a given thermodynamic environment, more updraft mass flux and, more specifically, more hydrometeor production tend to yield more downdraft mass flux. While parameters such as DCAPE may be useful for predicting the negative buoyancy potential for individual downdraft parcels that remain saturated, it seems likely that the intensity of low-level convective outflow is highly dependent on the volume of mass produced, regardless of the evaporative cooling effects from individual parcels. The recent modeling results of James and Markowski (2010) support this idea. They find several measures of convective system strength (total rainfall, total mass of each condensate species, and total updraft and downdraft mass fluxes) to generally increase as low- to midlevel dryness is lessened for the midlatitude MCS environments modeled in their study.

f. Environmental wind shear after MCS development

The strong LLJ and rapidly evolving wind field produced a complex wind shear environment, which was a large part of what made this environment so different from those typically used in the MCS modeling literature [see Weisman and Rotunno (2004), Stensrud et al. (2005), and Bryan et al. (2006) for a review]. For typical MCS cold pools in the central United States (Engerer et al. 2008), the amount of shear needed to support organized, severe MCSs in typical modeling frameworks is substantial (roughly greater than 15–20 m s^{-1}) but is generally found to exist over the lowest 6 km or so in MCS environments (Bluestein and Jain 1985; Johns 1993; Evans and Doswell 2001; Coniglio et al. 2004; Cohen et al. 2007).

Indeed, substantial 0–6-km shear was found in the 8 May 2009 environment, with values increasing from about

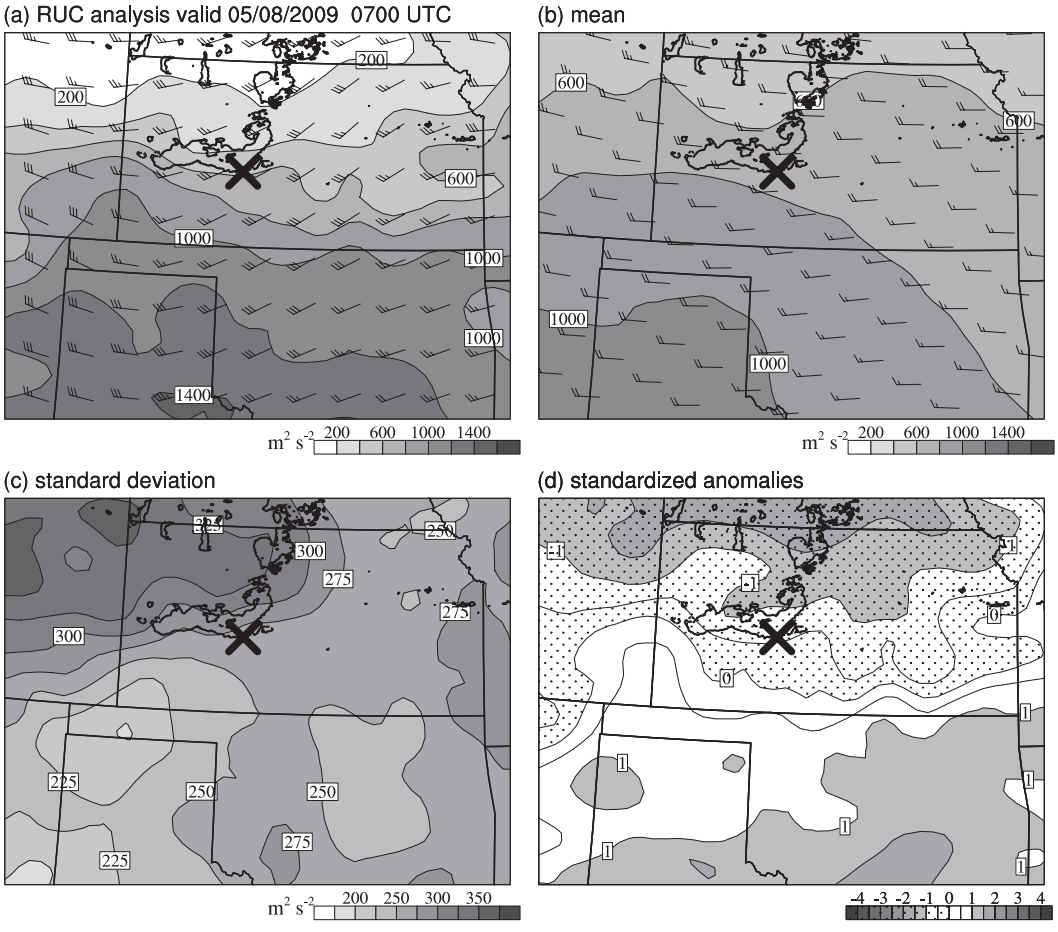

FIG. 19. As in Fig. 16, but for DCAPE (shaded and contoured every 200 $m^2\ s^{-2}$) and 0–6-km mean wind vectors (full barb = 5 $m\ s^{-1}$, pennant = 25 $m\ s^{-1}$) valid at 0700 UTC 8 May 2009.

20 $m\ s^{-1}$ ahead of the southern end of the system to over 30 $m\ s^{-1}$ ahead of the northern half of the system (Fig. 20a), much of which is found in the 3–6-km layer[4] (Fig. 18a). However, while the 0–6-km shear values are above the mean (Fig. 20d), the standardized anomalies (0.5–1.5) were not as high as those found for both the LLJ (Fig. 16d) and the thermodynamic variables shown earlier. Similarly, the mean wind speeds over various layers in the environment (see the vectors plotted in Fig. 19 for the 0–6-km mean wind) were not unusually large (not shown).

This suggests that the unusually strong, deep, and extensive LLJ and its import of air with extremely high moisture content (Fig. 17), and the development of very large mid-level lapse rates, set this MCS apart from the others in C2010 more so than the strength of the environmental flow or vertical wind shear.

Furthermore, the shear vectors display large variability both temporally (Figs. 14 and 15) and spatially (see Fig. 17a for the 0–3-km shear vectors, Fig. 18a for the 3–6-km shear vectors, and Fig. 20a for the 0–6-km shear vectors). This prevents a definitive assessment on the impacts of the shear on the MCS evolution, particularly as it applies to cold pool–shear balance ideas (Weisman and Rotunno 2004). This topic of highly variable shear for the 8 May 2009 event is the subject of an ongoing investigation and will be detailed in a companion paper to be submitted soon.

4. Summary and concluding remarks

This study documents the development and early evolution of the remarkable derecho-producing MCS that

[4] The 3–6-km shear values ranged from 10 to 20 $m\ s^{-1}$ ahead of the MCS (Fig. 17a). Substantial shear *based* at 2 or 3 km is a characteristic of the environment that separates long-lived MCSs from short-lived MCSs in the C2010 dataset. The effects of shear and strong flow above the cold pool on the evolution of convective systems are not clear, but it could allow the updrafts to remain along the leading edge of the cold pool for longer periods (Parker and Johnson 2004; Coniglio et al. 2006) or provide a source of westerly momentum to be transferred to the surface in the cold pool (Corfidi 2003; Mahoney et al. 2009).

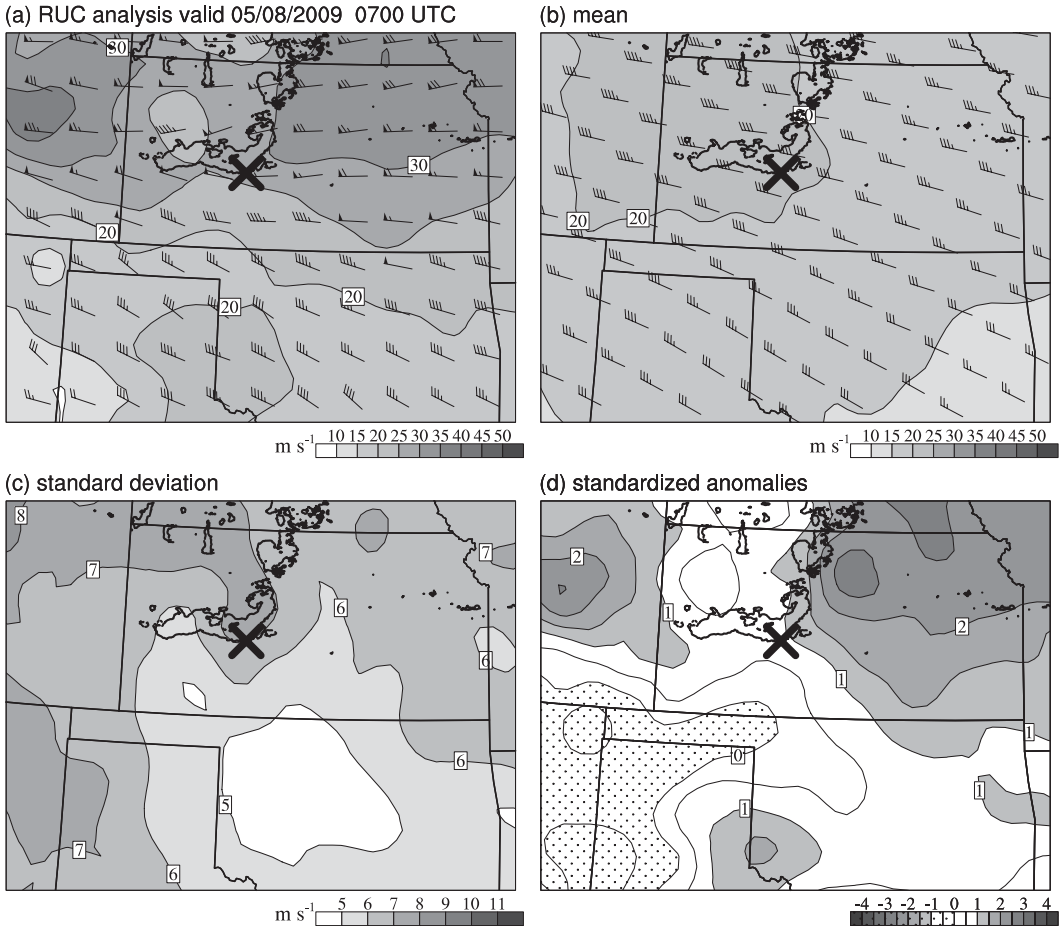

FIG. 20. As in Fig. 16, but for the 0–6-km wind shear magnitude (shaded and contoured every 5 m s^{-1}) and 0–6-km wind shear vectors (full barb = 5 m s^{-1}, pennant = 25 m s^{-1}) valid at 0700 UTC 8 May 2009.

traversed the central United States on 8 May 2009. The goal is to show that the evolution of the storms and the environment leading up to the development of the derecho was very complex, but the potential for a particularly severe convective wind event was signaled by strong anomalies in the prestorm environment. Given the complexity of the convective evolution, and the departure it represents from the cleaner and simpler environments that are the focus of the MCS modeling literature, unraveling the evolution that led to the severity of this event is no easy task. However, examination of the anomalies in the environment and the evolving convective morphology yields important clues about the processes that shaped this event and led to a successful prediction of an extreme damaging-wind event.

Initial convective development in northeastern Colorado was fairly weak and unremarkable, but when outflow from some of these weaker storms began to lift slightly more unstable low-level air in western Kansas, a line of more intense convection developed. Meanwhile, a deep layer of warm moist air surged northward out of Oklahoma and into the path of this initial line. Multiple features in the environment, possibly associated with airmass boundaries along the leading edge of this surge, appeared to trigger several new convective lines in south-central and southeastern Kansas, including at least two bands with a distinctly different orientation than the initial line. Eventually, these components consolidated into a large MCS with a clear MCV and a strongly bowing convective line on the southeastern flank. Although damaging winds were produced during the bowing stage of the system, a remarkable aspect of this event (but one that is not the focus of this study) was the very strong and long-lived MCV that persisted for several hours after the weakening of the main convective line.

The magnitude and geographical extent of severe winds associated with this event were anomalous compared to other MCSs. Yet, while the winds in the early evolution of the MCS were associated with convective downdrafts, commonly used methods to estimate the

strength of convective downdraft outflow based on environmental parameters did not yield unusually high values compared to other MCSs. Although the 0–6-km wind shear and mean wind speeds were certainly sufficient for organized severe convection and surface outflow, the values were not exceptionally large compared to other central plains MCS environments. Furthermore, the low-level shear profile was found to be very complex and highly variable throughout the evolution of the event through the bow-echo stage, and prevented a clear application of cold pool–low-level shear balance ideas to this event.

However, consideration of those environmental parameters that were unusual and consistent has important implications for predicting the strength of the downdraft outflow, by virtue of what these parameters say about updrafts. For example, anomalously strong fields in this event include low-level storm inflow, PW, conditional instability, and inertial instability aloft. The combination of these multiple factors suggests that intense upward mass fluxes were strongly favored in this event: the potential energy supply was high, the relative humidity was high over deep layers favoring minimal dilution of updrafts by entrainment, and an upper-tropospheric environment that could accommodate massive detrainment of mass was present.

Why are these factors important for downdrafts? In a given thermodynamic environment, more updraft mass flux and, more specifically, more hydrometeor production tend to yield more downdraft mass flux. Therefore, factors that support large updraft mass fluxes in a concentrated area, like the combination of high PW, a very strong and deep LLJ, and very steep lapse rates, like those found in this study, can also influence the strength of the convective downdrafts, regardless of the evaporation potential. This hypothesis for the 8 May 2009 derecho seems to be consistent with the results of James and Markowski (2010). They show that simulated MCSs generally become weaker as the low- to midlevel dryness is increased for the midlatitude MCS environments modeled in their study. They explain that the increased entrainment of drier air into the updrafts reduces hail production and reduces the associated downdraft mass fluxes and outflow winds, and is a primary reason for the weaker MCSs.

Environmental parameters and observations of radar reflectivity indicate that an extraordinary amount of hydrometeors was available to drive downdrafts. Even though the potential energy for individual downdraft parcels was not exceptionally large, it seems likely that the enormous updraft mass flux, resulting from a very strong and deep LLJ, very large lapse rates, and high PW in a confined area, led to high concentrations of hydrometeors that supported large downdraft mass fluxes, regardless of the evaporative potential. Water loading and/or the melting of abundant frozen hydrometeors aloft likely played an important role in producing the downdraft mass fluxes in this environment, since the evaporative potential was not exceptionally high. These processes are perhaps underappreciated in severe nocturnal MCS events.

Acknowledgments. Part of the analysis presented herein stemmed from discussions at the QLCS Advanced Warning Operations Course (AWOC) developers workshop run by the NOAA/NWS/Warning Decision Training Branch (WDTB). Participants included Ron Przybylinski, the science and operations officer (SOO) at the NWS Forecast Office (WFO) in St. Louis, Missouri; Ray Wolf, SOO at the Davenport, Iowa, WFO; Dan Miller, SOO at the Duluth, Minnesota, WFO; Pat Spoden, SOO at the Paducah, Kentucky, WFO; Angela Lese from the WFO in Louisville, Kentucky; Jeff Evans from the SPC; Dr. Nolan Atkins from Lyndon State College; and Brad Grant, Jim LaDue, Steve Martinaitis, Les Lemon, and Chris Spannagle from the WDTB. A discussion with Dan Miller about the role of frontogenesis in MCS environments was helpful. Patrick Marsh of the OU School of Meteorology helped with the interpretation of WSR-88D level II data in the Gibson Ridge GR2Analyist software. Greg Carbin of the NOAA/Storm Prediction Center provided the data on PDS severe thunderstorm watches and inspired the authors to present the hourly composite reflectivity in one image (Fig. 1a). Jason Levit, Andy Dean, and Jay Liang of the SPC archived the SPC operational data stream for this case, which allowed for an efficient perusal of the data for this study. Finally, we thank Dr. Matthew Parker for his very thorough reviews of this manuscript and many helpful suggestions along the way, as well as Drs. David Stensrud, Mace Bentley, and David Schultz for their helpful comments and suggestions on earlier versions of this manuscript.

REFERENCES

Adams-Selin, R. D., and R. H. Johnson, 2010: Mesoscale surface pressure and temperature features associated with bow echoes. *Mon. Wea. Rev.,* **138,** 212–227.

Atkins, N. T., and M. St. Laurent, 2009: Bow echo mesovortices. Part I: Processes that influence their damaging potential. *Mon. Wea. Rev.,* **137,** 1497–1513.

Benjamin, S. G., and Coauthors, 2004: An hourly assimilation–forecast cycle: The RUC. *Mon. Wea. Rev.,* **132,** 495–518.

Bentley, M. L., and J. M. Sparks, 2003: A 15 yr climatology of derecho-producing mesoscale convective systems over the central and eastern United States. *Climate Res.,* **24,** 129–139.

Blackadar, A. K., 1957: Boundary layer wind maxima and their significance for the growth of nocturnal inversions. *Bull. Amer. Meteor. Soc.,* **38,** 283–290.

Blanchard, D. O., W. R. Cotton, and J. M. Brown, 1998: Mesoscale circulation growth under conditions of weak inertial instability. *Mon. Wea. Rev.,* **126,** 118–140.

Bluestein, H. B., and M. H. Jain, 1985: Formation of mesoscale lines of precipitation: Severe squall lines in Oklahoma during the spring. *J. Atmos. Sci.,* **42,** 1711–1732.

Bonner, W. D., 1968: Climatology of the low-level jet. *Mon. Wea. Rev.,* **96,** 833–850.

Bryan, G. H., D. A. Ahijevych, C. Davis, S. B. Trier, and M. L. Weisman, 2005: Observations of cold pool properties in mesoscale convective systems during BAMEX. Preprints, *32nd Conf. on Mesoscale Meteorology/11th Conf. on Mesoscale Processes,* Albuquerque, NM, Amer. Meteor. Soc., JP5J.12. [Available online at http://ams.confex.com/ams/pdfpapers/96718.pdf.]

——, J. C. Knievel, and M. D. Parker, 2006: A multimodel assessment of RKW theory's relevance to squall-line characteristics. *Mon. Wea. Rev.,* **134,** 2772–2792.

Burke, P. C., and D. M. Schultz, 2004: A 4-yr climatology of cold-season bow echoes over the continental United States. *Wea. Forecasting,* **19,** 1061–1074.

Cohen, A. E., M. C. Coniglio, S. F. Corfidi, and S. J. Corfidi, 2007: Discrimination of mesoscale convective system environments using sounding observations. *Wea. Forecasting,* **22,** 1045–1062.

Coniglio, M. C., and D. J. Stensrud, 2004: Interpreting the climatology of derechos. *Wea. Forecasting,* **19,** 595–605.

——, ——, and M. B. Richman, 2004: An observational study of derecho-producing convective systems. *Wea. Forecasting,* **19,** 320–337.

——, ——, and L. J. Wicker, 2006: Effects of upper-level shear on the structure and maintenance of strong quasi-linear convective systems. *J. Atmos. Sci.,* **63,** 1231–1252.

——, J. Y. Hwang, and D. J. Stensrud, 2010: Environmental factors in the upscale growth and longevity of MCSs derived from Rapid Update Cycle analyses. *Mon. Wea. Rev.,* **138,** 3514–3539.

Corfidi, S. F., 2003: Cold pools and MCS propagation: Forecasting the motion of downwind-developing MCSs. *Wea. Forecasting,* **18,** 997–1017.

Cotton, W. R., M. S. Lin, R. L. McAnelly, and C. J. Tremback, 1989: A composite model of mesoscale convective complexes. *Mon. Wea. Rev.,* **117,** 765–783.

Davis, C. A., and S. B. Trier, 2007: Mesoscale convective vortices observed during BAMEX. Part I: Kinematic and thermodynamic structure. *Mon. Wea. Rev.,* **135,** 2029–2049.

Durran, D. R., 1986: Mountain waves. *Mesoscale Meteorology and Forecasting,* P. S. Ray, Ed., Amer. Meteor. Soc., 472–492.

Emanuel, K. A., 1979: Inertial instability and mesoscale convective systems. Part I: Linear theory of inertial instability in rotating viscous fluids. *J. Atmos. Sci.,* **36,** 2425–2449.

Engerer, N. A., D. J. Stensrud, and M. C. Coniglio, 2008: Surface characteristics of observed cold pools. *Mon. Wea. Rev.,* **136,** 4839–4849.

Evans, J. S., and C. A. Doswell III, 2001: Examination of derecho environments using proximity soundings. *Wea. Forecasting,* **16,** 329–342.

French, A. J., and M. D. Parker, 2010: The response of simulated nocturnal convective systems to a developing low-level jet. *J. Atmos. Sci.,* **67,** 3384–3408.

Fujita, T. T., 1978: Manual of downburst identification for Project NIMROD. SMRP Research Paper 156, University of Chicago, 104 pp.

Houze, R. A., Jr., S. A. Rutledge, M. I. Biggerstaff, and B. F. Smull, 1989: Interpretation of Doppler weather radar displays of midlatitude mesoscale convective systems. *Bull. Amer. Meteor. Soc.,* **70,** 608–619.

James, R. P., and P. M. Markowski, 2010: A numerical investigation of the effects of dry air aloft on deep convection. *Mon. Wea. Rev.,* **138,** 140–161.

——, J. M. Fritsch, and P. M. Markowski, 2005: Environmental distinctions between cellular and slabular convective lines. *Mon. Wea. Rev.,* **133,** 2669–2691.

Jirak, I. L., and W. R. Cotton, 2003: Satellite and radar survey of mesoscale convective system development. *Mon. Wea. Rev.,* **131,** 2428–2449.

Johns, R. H., 1993: Meteorological conditions associated with bow echo development in convective storms. *Wea. Forecasting,* **8,** 294–299.

——, and W. D. Hirt, 1987: Derechos: Widespread convectively induced windstorms. *Wea. Forecasting,* **2,** 32–49.

Laing, A. G., and J. M. Fritsch, 2000: The large-scale environments of the global populations of mesoscale convective complexes. *Mon. Wea. Rev.,* **128,** 2756–2776.

Maddox, R. A., 1983: Large-scale conditions associated with mid-latitude, mesoscale convective complexes. *Mon. Wea. Rev.,* **111,** 1475–1493.

Mahoney, K. M., G. M. Lackmann, and M. D. Parker, 2009: The role of momentum transport in the motion of a quasi-idealized mesoscale convective system. *Mon. Wea. Rev.,* **137,** 3316–3338.

McAnelly, R. L., J. E. Nachamkin, W. R. Cotton, and M. E. Nicholls, 1997: Upscale evolution of MCSs: Doppler radar analysis and analytical investigation. *Mon. Wea. Rev.,* **125,** 1083–1110.

McNider, R. T., and R. A. Pielke, 1981: Diurnal boundary-layer development over sloping terrain. *J. Atmos. Sci.,* **38,** 2198–2212.

Miller, D. J., and R. H. Johns, 2000: A detailed look at extreme wind damage in derecho events. Preprints, *20th Conf. on Severe Local Storms,* Orlando, FL, Amer. Meteor. Soc., 52–55.

Orlanski, I., 1975: A rational sub-division of scales for atmospheric processes. *Bull. Amer. Meteor. Soc.,* **56,** 527–530.

Parker, M. D., 2008: Response of simulated squall lines to low-level cooling. *J. Atmos. Sci.,* **65,** 1323–1341.

——, and R. H. Johnson, 2000: Organizational modes of mid-latitude mesoscale convective systems. *Mon. Wea. Rev.,* **128,** 3413–3436.

——, and ——, 2004: Structures and dynamics of quasi-2D mesoscale convective systems. *J. Atmos. Sci.,* **61,** 545–567.

Richardson, Y. P., K. K. Droegemeier, and R. P. Davies-Jones, 2007: The influence of horizontal environmental variability on numerically simulated convective storms. Part I: Variations in vertical shear. *Mon. Wea. Rev.,* **135,** 3429–3455.

Rotunno, R., J. B. Klemp, and M. L. Weisman, 1988: A theory for strong, long-lived squall lines. *J. Atmos. Sci.,* **45,** 463–485.

Schultz, D. M., and P. N. Schumacher, 1999: The use and misuse of conditional symmetric instability. *Mon. Wea. Rev.,* **127,** 2709–2732; Corrigendum, **128,** 1573.

——, and J. A. Knox, 2007: Banded convection caused by frontogenesis in a conditionally, symmetrically, and inertically unstable environment. *Mon. Wea. Rev.,* **135,** 2095–2110.

Seman, C. J., 1994: A numerical study of nonlinear nonhydrostatic conditional symmetric instability in a convectively unstable atmosphere. *J. Atmos. Sci.,* **51,** 1352–1371.

Stensrud, D. J., M. C. Coniglio, R. P. Davies-Jones, and J. S. Evans, 2005: Comments on "'A theory for strong long-lived squall lines' revisited." *J. Atmos. Sci.,* **62,** 2989–2996.

Szoke, E., M. Weisman, J. Brown, F. Caracena, and T. Schlatter, 1984: A subsynoptic analysis of the Denver tornadoes of 3 June 1981. *Mon. Wea. Rev.,* **112,** 790–808.

Trier, S. B., C. A. Davis, D. A. Ahijevych, M. L. Weisman, and G. H. Bryan, 2006: Mechanisms supporting long-lived episodes of propagating nocturnal convection within a 7-day WRF model simulation. *J. Atmos. Sci.,* **63,** 2437–2461.

Tuttle, J. D., and C. A. Davis, 2006: Corridors of warm season precipitation in the central United States. *Mon. Wea. Rev.,* **134,** 2297–2317.

Uccellini, L. W., and D. R. Johnson, 1979: The coupling of upper and lower tropospheric jet streaks and implications for the development of severe convective storms. *Mon. Wea. Rev.,* **107,** 682–703.

Vasiloff, S. V., and Coauthors, 2007: Improving QPE and very short term QPF: An initiative for a community-wide integrated approach. *Bull. Amer. Meteor. Soc.,* **88,** 1899–1911.

Weisman, M. L., 1993: The genesis of severe, long-lived bow echoes. *J. Atmos. Sci.,* **50,** 645–670.

——, and R. Rotunno, 2004: ''A theory for strong, long-lived squall lines'' revisted. *J. Atmos. Sci.,* **61,** 361–382.

Wheatley, D. M., R. J. Trapp, and N. T. Atkins, 2006: Radar and damage analysis of severe bow echoes during BAMEX. *Mon. Wea. Rev.,* **134,** 791–806.

Zipser, E. J., 1982: Use of a conceptual model of the life cycle of mesoscale convective systems to improve very-short-range forecasts. *Nowcasting,* K. Browning, Ed., Academic Press, 191–221.